CrossMark
click for updates

Spin-phonon coupling in antiferromagnetic nickel oxide

E. Aytan,[1,2] B. Debnath,[3] F. Kargar,[1,2] Y. Barlas,[3] M. M. Lacerda,[2,4] J. X. Li,[5] R. K. Lake,[3,6] J. Shi,[5,6] and A. A. Balandin[1,6,a]

[1]Nano-Device Laboratory (NDL), Department of Electrical and Computer Engineering, University of California, Riverside, California 92521, USA
[2]Phonon Optimized Engineered Materials (POEM) Center, Materials Science and Engineering Program, University of California, Riverside, California 92521, USA
[3]Laboratory for Terascale and Terahertz Electronics (LATTE), Department of Electrical and Computer Engineering, University of California, Riverside, California 92521, USA
[4]Campus Duque de Caxias, Universidade Federal do Rio de Janeiro, Duque de Caxias, RJ 25245-390, Brazil
[5]Department of Physics and Astronomy, University of California, Riverside, California 92521, USA
[6]Spins and Heat in Nanoscale Electronic Systems (SHINES) Center, University of California, Riverside, California 92521, USA

We report the results of ultraviolet Raman spectroscopy of NiO, which allowed us to determine the spin-phonon coupling coefficients in this important antiferromagnetic material. The use of the second-order phonon scattering and ultraviolet laser excitation ($\lambda = 325$ nm) was essential for overcoming the problem of the optical selection rules and dominance of the two-magnon band in the visible Raman spectrum of NiO. We established that the spins of Ni atoms interact more strongly with the longitudinal than transverse optical phonons and produce opposite effects on the phonon energies. The peculiarities of the spin-phonon coupling are consistent with the trends given by density functional theory. The obtained results shed light on the nature of the spin-phonon coupling in antiferromagnetic insulators and can help in developing spintronic devices. *Published by AIP Publishing.*
https://doi.org/10.1063/1.5009598

Nickel oxide (NiO) has been studied extensively for various applications ranging from electrochemistry to solar cells.[1,2] In recent years, NiO attracted much attention as an antiferromagnetic (AF) insulator material for spintronic devices.[3–11] Understanding the spin-phonon coupling in NiO is a key to its functionalization and enabling AF spintronics' promise of ultra-high-speed and low-power dissipation.[12,13] The use of spin currents in spintronic devices instead of charge currents in electronic devices is advantageous for ultra-low energy dissipation.[12,13] NiO occupies a special role among spintronic AF insulator materials.[4–9] Its high Néel temperature, $T_N = 523$ K, allows for device operation in the AF state at room temperature (RT) and above. The demonstrated coherent THz control of AF spin waves suggests a possibility of ultra-high speed operation of NiO spintronic devices. NiO has been used for spin-fluctuation mediated transmission of spin current.[3] Unlike in ferromagnetic (FM) materials, an external magnetic field does not cause significant change in the static spin structure or spin wave excitations in NiO,[14] which is a major benefit for spintronic memory and logic applications.

However, despite its status as an exemplary AF insulator and a benchmark material for the study of correlated electron systems, little is known about the spin-phonon interaction and the associated energy dissipation channel in NiO. This gap in knowledge is explained by NiO optical selection rules, high Néel temperature, and dominance of the magnon band in the visible Raman spectrum, which precludes a conventional approach for investigating such an interaction. In

addition, there is a long-standing controversy over the large discrepancies between the experimental and theoretical values for the electron, phonon, and magnon energies in NiO.[15–25] It has been suggested that the spin-phonon interaction is likely behind this discrepancy, although no direct proof has been offered. The importance of the knowledge of the spin-phonon coupling in NiO goes beyond fundamental science owing to its relevance to magnon damping in spin wave devices.

The strength of the spin-phonon coupling in many FM and AF materials, e.g., FeF_2, MnF_2, and NiF_2, has been determined from the spectral position of the phonon peaks in the Raman spectra taken over wide temperature ranges extending below and above the Néel temperature T_N.[26–31] The deviation of the phonon peak position below T_N from the theoretically predicted phonon anharmonic decay curve was attributed to the effects of spin texture on the phonon energies.[26–31] The anharmonic decay dependence was obtained from theory fitting to experimental data points above T_N. This conventional method does not work for NiO for several specific reasons. The first-order longitudinal optical (LO) and transverse optical (TO) phonons are not Raman active in rock-salt crystals.[32] A weak rhombohedral lattice distortion in NiO below T_N or the presence of defects can make LO and TO phonons visible in the Raman spectrum but their low intensity does not allow for the extraction of the coupling strength. The second-order LO and TO bands, denoted as 2LO and 2TO, have much higher intensity but always appear within the large background of the second-order two-magnon (2M) band, which does not permit an accurate phonon peak position analysis.[15,16,21,33,34] Moreover, because the Néel temperature in NiO is very high ($T_N = 523$ K), there is a limited temperature

range above T_N available for fitting to the anharmonic curve, before irreversible structural changes start to happen to the NiO crystal lattice.[25] All of these factors together make the study of spin-phonon interactions in NiO challenging.

We employed UV Raman spectroscopy, which allows for the suppression of the 2M band, to overcome the above mentioned difficulties and determine the spin coupling with LO and TO phonons. The single crystal NiO slab samples, selected for this study, have the crystalline growth plane oriented in the [111] direction. The X-ray diffraction (XRD) inspection confirmed their high quality. NiO has a two-sub-lattice AF crystalline structure consisting of FM aligned (111) planes that are AF aligned with respect to each other.[4,8,9] The AF ordering of NiO is due to the super-exchange interaction mediated by O orbitals.[33] Above T_N, NiO has a face-centered cubic (FCC) structure with paramagnetic (PM) ordering, while below T_N, the NiO lattice is characterized by a weak rhombohedral distortion.[35]

Raman spectroscopy (Renishaw InVia) was performed in the backscattering configuration under visible (2.54 eV or 488 nm) and UV (3.81 eV or 325 nm) laser excitation. The excitation laser power was limited to 2 mW to avoid any possible effects on the sample surface due to local heating. Spectra at different temperatures were measured with the sample in a cold-hot cell with a constant flow of pure Ar gas to avoid surface oxidation. The temperature, T, was accurately controlled at each step. The sample was heated or cooled to a certain T and then maintained at that T for ~10 min to ensure that the entire sample reached a constant T. Figures 1(a) and 1(b) show the room temperature (RT) Raman spectrum of NiO under visible and UV excitation. The weak peaks observed in the range from $350\,cm^{-1}$ to $410\,cm^{-1}$ and from $520\,cm^{-1}$ to $580\,cm^{-1}$ are the TO and LO phonon modes, respectively. The stronger second-order peaks are assigned to 2TO (~$738\,cm^{-1}$), 2LO ($1142\,cm^{-1}$), and a combination of TO + LO ($913\,cm^{-1}$) phonon modes, which is consistent with the literature.[15,21,36] The spectral positions are given for UV Raman spectra, which may deviate from those in visible Raman spectra due to the difference in the probing phonon wave vector $k_p = 4\pi fn/c$ and possible resonant excitation effects for the compositional peaks (here, f is the excitation frequency, c is the speed of light, and n is the refractive index of the material at given frequency). The probing phonon wave vector for UV laser excitation is $k_p = 0.124\,nm^{-1}$, which is approximately twice of that for the visible. The second-order 2M peak around $1500\,cm^{-1}$ is a dominant feature of the visible Raman spectrum. It originates from two Brillouin zone (BZ) edge magnons, likely X or Z points, propagating with opposite momenta.[19,37] There are always substantial deviations in the measured and theoretically predicted energies of the 2M band, likely related to the spin-phonon coupling. The most striking feature of the UV Raman spectrum is the absence of the 2M band.

The suppression of the 2M band is likely related to the resonant excitation effects. Our observation is in agreement with the report of the absolute Raman scattering cross-section, S, in NiO.[38] It was found that S experiences a maximum at the excitation energy of ~2.1 eV and then rapidly decreases by more than an order-of-magnitude for the excitation above ~2.6 eV.[38] The UV excitation energy that we
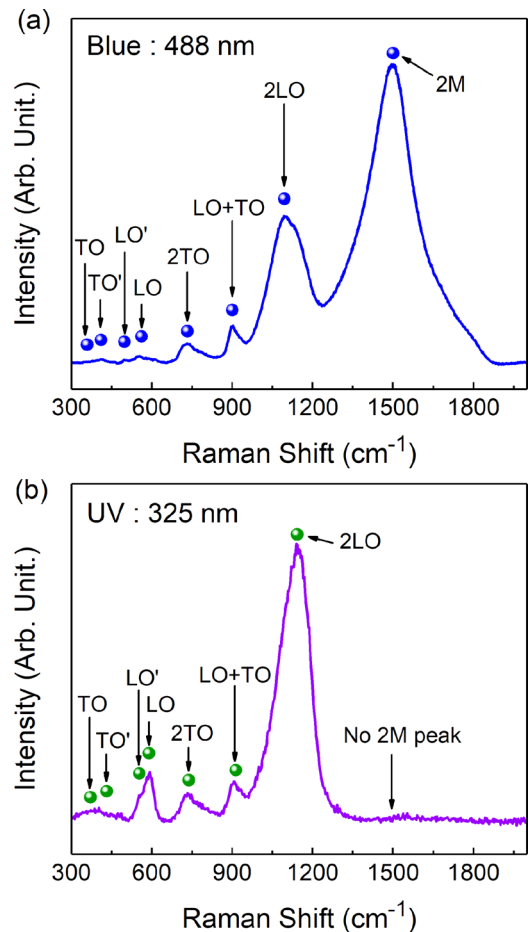

FIG. 1. The room-temperature backscattering spectra are shown for (a) 488 nm and (b) 325 nm laser excitation. The labeled spheres indicate the position of the first-order and second-order Raman peaks.

selected (3.81 eV) is close to the NiO optical bandgap energy $E_G = 3.80\,eV$ measured by the reflectance studies.[39,40] The exact E_G value is a non-trivial question for NiO since the reported energies vary from 3.5 eV to 4.3 eV.[39–41] Matching the resonant band-to-band transition increases the light absorption while simultaneously enhancing the phonon Raman peaks near the Γ point. The increased light absorption leads to decreased penetration depth and reduced interaction volume, which, in turn, translates to the smaller peak intensities unless compensated by the resonant enhancement. The resonant conditions for the Γ-point 2LO phonons and the BZ-edge 2M band[19,37,42] can differ, which may affect the Raman intensities. The excitation of the electron–hole pairs due to light absorption can also influence the scattering processes. The important consequence for the present work is that the absence of the strong 2M background allowed us to accurately determine the 2LO and 2TO band temperature dependence.

To elucidate the spin-phonon interaction in NiO, we conducted UV Raman spectroscopy for temperatures below and above T_N. Figures 2(a) and 2(b) show the evolution of 2TO and 2LO peaks over a wide temperature range. We were careful to keep the temperature below ~700 K to avoid any irreversible structural changes with the material.[25] Below T_N, the phonon peak position is affected by the AF spin texture.[43] Thus, in order to determine the strength of the
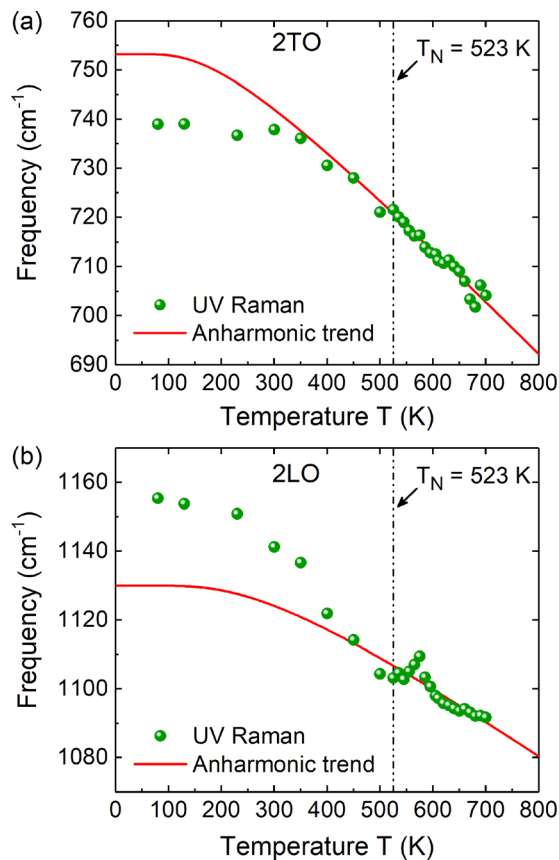
FIG. 2. Temperature dependence of the frequencies of the second-order (a) 2TO and (b) 2LO Raman-active phonons in NiO. The spheres indicate all measured Raman peaks at different temperatures whereas the lines show the theoretical anharmonic trend for NiO fitted for the experimental data points above T_N. The difference of Raman peaks and anharmonic lines at low temperature is directly proportional to the spin-phonon coupling constant. Note that the spin-phonon coupling produces an opposite effect on the TO and LO phonon energies in NiO.

spin-phonon coupling, one needs to separate it from the baseline temperature dependence due to the crystal lattice anharmonicity. The anharmonic dependence of the phonon frequency is given within second-order perturbation theory as,[44,45] $\omega_A(T) = \omega(0) - A(1 + 2/(e^{\frac{\hbar\omega(0)}{2K_BT}} - 1))$, where A and $\omega(0)$ are the fitting constants, while $\omega_A(T)$ is the phonon frequency determined by the anharmonicity alone. The experimental data points at temperatures $T > T_N$, where NiO becomes PM, but lower than ~700 K, are those that should be used for fitting with the goal of determining the anharmonic phonon decay baseline. One can see that there is a significant deviation of the experimental data points below T_N from this dependence, indicating a strong spin-phonon coupling in NiO.

The renormalized phonon frequency, ω_R, due to the spin-dependent effects is given as[26,28,46] $\omega_R = \omega_0 + \lambda \langle S_i \cdot S_j \rangle$. Here, ω_0 denotes the phonon frequency in the absence of spin correlations, and $\langle S_i \cdot S_j \rangle$ is the spin-spin correlation function of the adjacent spins. For $T > T_N$, the spin correlation function approaches to zero, terminating any spin-phonon effect in the paramagnetic phase, i.e., $\omega_R \rightarrow \omega_0$. Hence, the spin-phonon coupling constant λ is proportional to the difference in the frequency between the two phases, $\Delta\omega = (\omega_R - \omega_0)$. From this deviation, we calculated the spin-phonon coupling

factors, λ, for TO and LO phonons as -7.9 cm^{-1} and 14.1 cm^{-1}, respectively. The AF spin texture in NiO results in substantial softening of the TO phonon and hardening of the LO phonon. For comparison, the spin-phonon coupling in NiO is substantially stronger than that in other common AF materials such as MnF$_2$ ($\lambda = 0.4$ cm^{-1}),[26] FeF$_2$ ($\lambda = 1.3$ cm^{-1}),[26] or ZnCr$_2$O$_4$ ($\lambda = 3.2$ cm^{-1}, -6.2 cm^{-1})[46] although not as strong as in NaOsO$_3$ ($\lambda \sim 40$ cm^{-1})[47] and CuO ($\lambda \sim 50$ cm^{-1}),[48] which is perhaps the strongest reported to date. The measured spin-phonon coupling is for the AF direction of NiO. It is expected that this value will not change substantially for other directions.[49] In order to rationalize the obtained experimental results and understand if the strong spin-phonon coupling can be behind the observed discrepancy in the experimental and theoretical data for the phonon energies, we calculated the full phonon dispersion of NiO using *ab initio* density functional theory (DFT). Additional details of the calculations are provided in the supplementary material.

Figures 3(a) and 3(b) show the phonon dispersion of AF NiO and non-magnetic NiO (i.e., no spin ordering), respectively. The calculations were performed for the primitive cell containing two Ni atoms and two O atoms. The corresponding BZ is shown in Fig. 4(a). The x-axis labels in Figs. 3(a) and 3(b) are in the basis of the reciprocal lattice vectors of the AF primitive cell shown in Fig. 4(a). We used the
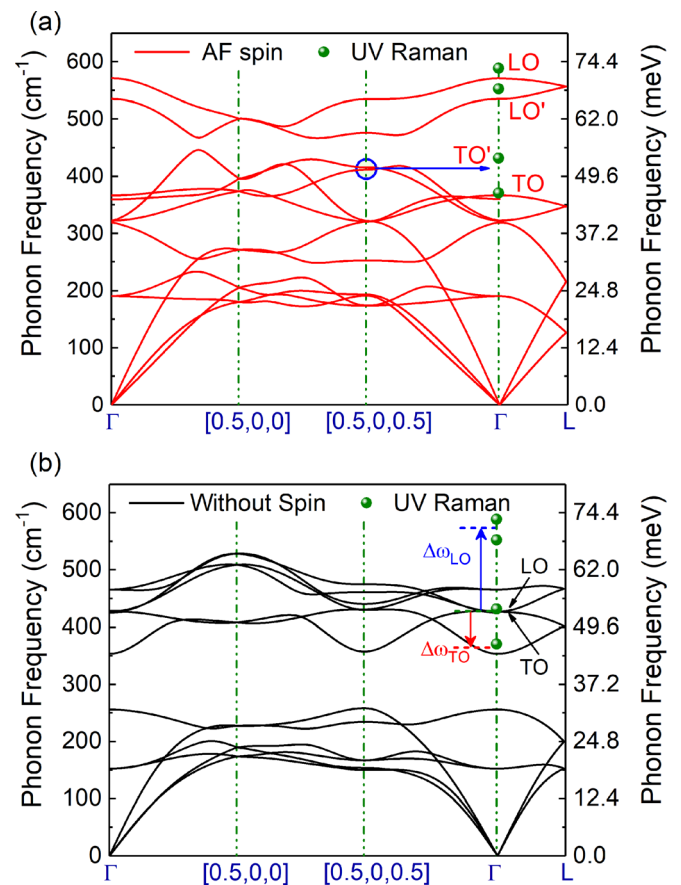

FIG. 3. (a) Phonon dispersion of NiO with AF spin texture. The spheres show the position of the measured UV Raman peaks. The TO' mode is a zone-folded manifestation of TO-like mode at $k = (0.5, 0, 0.5)$. (b) Phonon dispersion of NiO without spin texture. The blue and red arrows show the frequency shift, Δ, of the LO and TO phonon branches when AF spin ordering is included.
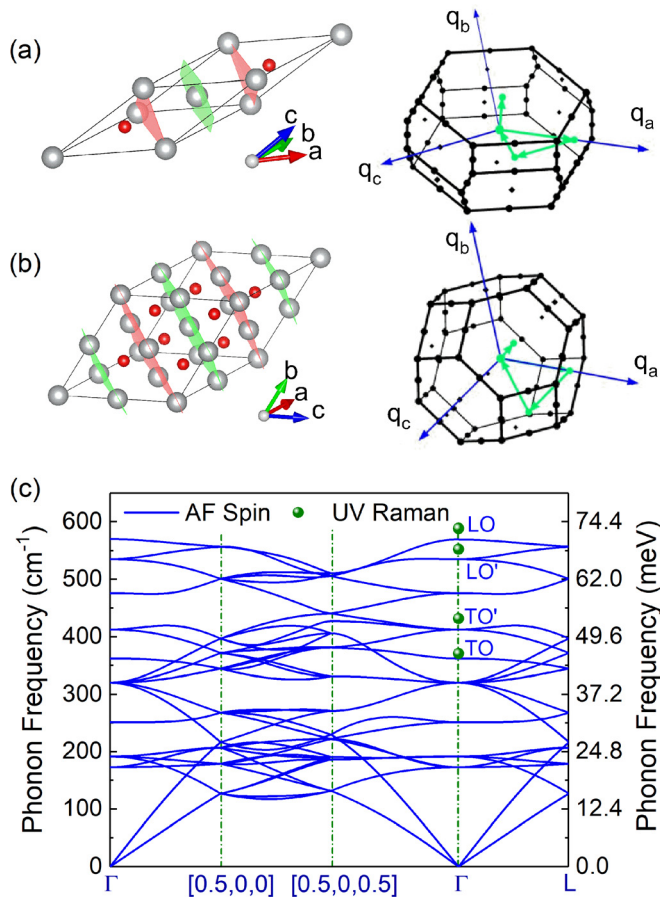
FIG. 4. (a) The AF primitive cell consisting of 2 Ni atoms (gray spheres) and 2 O atoms (red spheres), and corresponding Brillouin zone used for the calculations of Figs. 3(a) and 3(b). The green arrows indicate the BZ path direction. (b) The unit cell resulting from doubling the AF primitive cell and corresponding Brillouin zone. (c) The phonon dispersion resulting from the AF unit cell in (b). The zone-folding of the TO′ mode is apparent at Γ. Note a good agreement between the theory and experiment when the spin-phonon coupling is included.

non-orthogonal primitive unit-cells to reduce the number of atoms and required computation time in DFT calculations. We identify the first-order TO and LO modes from the corresponding atomic displacements. The positions of the experimental Raman peaks are indicated by the spheres. At the Γ point, the calculated frequencies of the slightly split TO mode are $360\,\mathrm{cm}^{-1}$ and $367\,\mathrm{cm}^{-1}$. The calculated TO mode splitting at the Γ point of $7\,\mathrm{cm}^{-1}$ depends on the BZ direction, and it is close to literature values.[43,50] The calculated frequencies of the LO′ and LO modes are at $535\,\mathrm{cm}^{-1}$ and $571\,\mathrm{cm}^{-1}$, respectively. Three of the calculated Γ-point phonon energies agree well with the UV Raman peaks, while the TO′ Raman peak at $413\,\mathrm{cm}^{-1}$ has no corresponding calculated energy at Γ. A comparison of the calculated LO and TO frequencies in Figs. 3(a) and 3(b) shows that the inclusion of AF spin texture hardens the LO phonon (increases the frequency) and softens the TO phonon (decreases the frequency). The calculated relative shift, $\Delta\omega$, is $-60.5\,\mathrm{cm}^{-1}$ and $146.2\,\mathrm{cm}^{-1}$ for TO and LO phonons, respectively. Hence, we expect that the spin phonon coupling of the LO phonon will be, approximately, two times larger in magnitude than that of the TO phonon, and the signs of the shifts will be opposite, specifically negative for the TO phonon and positive for the LO phonon. These trends in relative

magnitudes and signs are consistent with the experimental results [see Figs. 2(a) and 2(b)]. Our experimental results and *ab initio* calculations prove that inclusion of the spin-phonon interactions is essential for an accurate description of the phonon frequencies in NiO.

The experimental TO′ peak is absent in the DFT spectrum shown in Fig. 3(a); however, its source is indicated by the arrow. To better understand this feature, we double the size of the primitive cell in Fig. 4(a) to obtain the unit cell and corresponding BZ shown in Fig. 4(b). Performing the same phonon dispersion calculation for AF NiO with this unit cell gives the phonon dispersion shown in Fig. 4(c). The *x*-axis labels are in the basis of the reciprocal lattice vectors of the BZ in Fig. 4(b). We now observe that the experimental TO′ mode aligns with the calculated degenerate mode at Γ. To analyze this energy, we write the reciprocal lattice vectors of the larger unit cell in terms of those of the primitive unit cell to obtain $g'_a = \frac{1}{2}(g_a + g_b)$, $g'_b = \frac{1}{2}(g_a + g_c)$ and $g'_c = \frac{1}{2}(g_b + g_c)$. The *k*-point denoted as [0.5, 0, 0.5] $= \frac{1}{2}(g_a + g_c)$ in Figs. 3(a) and 3(b) lies at the center of the small face of the BZ in Fig. 4(a), and it is equal to g'_b in Fig. 4(b). Since the reciprocal lattice vectors correspond to equivalent Γ points, this *k*-point appears at Γ in Fig. 4(c). Thus, the calculated modes at the TO′ frequency originate from the center of the six small faces of the BZ of the AF primitive cell. An analysis of the atomic displacements of this mode shows that they are similar to the atomic displacements of the TO peak (see supplementary material, video). The theoretical approach can be further refined by calculating the phonon dispersion of the true PM phase NiO, which has random spin texture, and comparing the results with the AF phonon dispersion. This is a costly endeavor reserved for future study.

We now provide details of the extraction of the spin-phonon coupling coefficient, λ. It is calculated from the temperature-dependent UV Raman spectra. The frequency shift due to the spin-phonon coupling is given by $\Delta\omega_{sp-ph} = -\lambda S^2 \phi(T) = -\lambda\langle S_i \cdot S_j \rangle$, where ϕ is the short-range order parameter and S_i represents the spin of Ni atom site i. As the temperature goes beyond Néel temperature, T_N, the short-range spin ordering $\langle S_i \cdot S_j \rangle$ quickly falls off. The calculation of ϕ, using the mean field theory and the two-spin cluster theory, is already reported for $S = 2$ (FeF_2) and $S = 2.5$ (MnF_2).[26] Besides, prior results of ϕ of $S = 2$ have been used as a reasonable estimate of ϕ for $S = 1$ (Ni^{2+} in NiF_2),[28] mainly because ϕ does not change much with S. In our case, we make use of ϕ for Ni^{2+}, to extract the spin-phonon coupling factor, λ, in NiO using the expression

$$\lambda = -\frac{\omega_R(T_{low}) - \omega_A(T_{low})}{\left[\phi(T_{low}) - \phi(2T_N)\right] \cdot S^2}.$$

Here, $\omega_R(T_{low})$ is the observed Raman peak at the lowest temperature ($T_{low} \sim 80\,\mathrm{K}$) and $\omega_A(T_{low})$ is the anharmonic prediction of that Raman peak at $T = T_{low}$. According to the above equation, the calculated spin-phonon coupling factors, λ, for 2TO and 2LO modes are $-15.7\,\mathrm{cm}^{-1}$ and $28.2\,\mathrm{cm}^{-1}$. We divide the obtained λ of 2TO and 2LO by two, to get the λ for TO and LO modes, respectively. Since the second-order order peaks (2TO and 2LO) are more prominent in

Raman spectra, we use them to extract λ of TO and LO modes.

In conclusion, we determined the spin-phonon coupling in NiO using UV Raman spectroscopy. The coupling coefficients for TO and LO phonons in NiO were determined to be $-7.9\,cm^{-1}$ and $14.1\,cm^{-1}$, respectively. *Ab initio* calculations confirm that inclusion of spin texture is essential for obtaining the correct phonon energies and explaining the discrepancy in the data for NiO.[15–25,35,51–53] Our results have important implications for AF spintronics. Strong spin-phonon coupling provides a mechanism for optimizing spin wave propagation by tuning the phonon dispersion via geometrical confinement and strain. The knowledge of spin coupling to specific phonon polarizations can be important for minimizing the spin-wave damping.

See supplementary material for details of the DFT calculations; Raman spectrum analysis; and phonon mode assignments. The supplementary videos show vibrational modes in NiO.

[1]M. Gong, W. Zhou, M.-C. Tsai, J. Zhou, M. Guan, M.-C. Lin, B. Zhang, Y. Hu, D.-Y. Wang, J. Yang, S. J. Pennycook, B.-J. Hwang, and H. Dai, Nat. Commun. **5**, 4695 (2014).

[2]J. You, L. Meng, T.-B. Song, T.-F. Guo, Y. (Michael) Yang, W.-H. Chang, Z. Hong, H. Chen, H. Zhou, Q. Chen, Y. Liu, N. De Marco, and Y. Yang, Nat. Nanotechnol. **11**, 75 (2016).

[3]W. Lin, K. Chen, S. Zhang, and C. L. Chien, Phys. Rev. Lett. **116**, 186601 (2016).

[4]T. Kampfrath, A. Sell, G. Klatt, A. Pashkin, S. Mährlein, T. Dekorsy, M. Wolf, M. Fiebig, A. Leitenstorfer, and R. Huber, Nat. Photonics **5**, 31 (2011).

[5]U. Kaiser, A. Schwarz, and R. Wiesendanger, Nature **446**, 522 (2007).

[6]I. Sugiyama, N. Shibata, Z. Wang, S. Kobayashi, T. Yamamoto, and Y. Ikuhara, Nat. Nanotechnol. **8**, 266 (2013).

[7]T. Satoh, S.-J. Cho, R. Iida, T. Shimura, K. Kuroda, H. Ueda, Y. Ueda, B. A. Ivanov, F. Nori, and M. Fiebig, Phys. Rev. Lett. **105**, 77402 (2010).

[8]F. L. A. Machado, P. R. T. Ribeiro, J. Holanda, R. L. Rodríguez-Suárez, A. Azevedo, and S. M. Rezende, Phys. Rev. B **95**, 104418 (2017).

[9]C. Tzschaschel, K. Otani, R. Iida, T. Shimura, H. Ueda, S. Günther, M. Fiebig, and T. Satoh, Phys. Rev. B **95**, 174407 (2017).

[10]R. Khymyn, I. Lisenkov, V. Tiberkevich, B. A. Ivanov, and A. Slavin, Sci. Rep. **7**, 43705 (2017).

[11]T. F. Nova, A. Cartella, A. Cantaluppi, M. Först, D. Bossini, R. V. Mikhaylovskiy, A. V. Kimel, R. Merlin, and A. Cavalleri, Nat. Phys. **13**, 132 (2016).

[12]Y. Kajiwara, K. Harii, S. Takahashi, J. Ohe, K. Uchida, M. Mizuguchi, H. Umezawa, H. Kawai, K. Ando, K. Takanashi, S. Maekawa, and E. Saitoh, Nature **464**, 262 (2010).

[13]T. Jungwirth, X. Marti, P. Wadley, and J. Wunderlich, Nat. Nanotechnol. **11**, 231 (2016).

[14]J. Milano and M. Grimsditch, Phys. Rev. B **81**, 94415 (2010).

[15]R. E. E. Dietz, G. I. I. Parisot, and A. E. E. Meixner, Phys. Rev. B **4**, 2302 (1971).

[16]R. E. Dietz, W. F. Brinkman, A. E. Meixner, and H. J. Guggenheim, Phys. Rev. Lett. **27**, 814 (1971).

[17]M. T. Hutchings and E. J. Samuelsen, Phys. Rev. B **6**, 3447 (1972).

[18]R. A. Coy, C. W. Tompson, and E. Gürmen, Solid State Commun. **18**, 845 (1976).

[19]A. P. Cracknell and S. J. Joshua, Math. Proc. Cambridge Philos. Soc. **66**, 493–504 (1969).

[20]A. C. Gandhi, C.-Y. Huang, C. C. Yang, T. S. Chan, C.-L. Cheng, Y.-R. Ma, and S. Y. Wu, Nanoscale Res. Lett. **6**, 485 (2011).

[21]D. J. Lockwood, M. G. Cottam, and J. H. Baskey, J. Magn. Magn. Mater. **104–107**, 1053 (1992).

[22]M. Grimsditch, S. Kumar, and R. S. Goldman, J. Magn. Magn. Mater. **129**, 327 (1994).

[23]M. Grimsditch, L. E. McNeil, and D. J. Lockwood, Phys. Rev. B **58**, 14462 (1998).

[24]J. Milano, L. B. Steren, and M. Grimsditch, Phys. Rev. Lett. **93**, 77601 (2004).

[25]M. M. Lacerda, F. Kargar, E. Aytan, R. Samnakay, B. Debnath, J. X. Li, A. Khitun, R. K. Lake, J. Shi, and A. A. Balandin, Appl. Phys. Lett. **110**, 202406 (2017).

[26]D. J. Lockwood and M. G. Cottam, J. Appl. Phys. **64**, 5876 (1988).

[27]M. G. Cottam and D. J. Lockwood, *Light Scattering in Magnetic Solids* (Wiley-Interscience, 1986), ISBN-13: 978-047181701, ISBN-10: 0471817015.

[28]D. J. Lockwood, Low Temp. Phys. **28**, 505 (2002).

[29]J. Vermette, S. Jandl, and M. M. Gospodinov, J. Phys.: Condens. Matter **20**, 425219 (2008).

[30]Y. Sharma, S. Sahoo, W. Perez, S. Mukherjee, R. Gupta, A. Garg, R. Chatterjee, and R. S. Katiyar, J. Appl. Phys. **115**, 183907 (2014).

[31]E. Granado, A. García, J. A. Sanjurjo, C. Rettori, I. Torriani, F. Prado, R. D. Sánchez, A. Caneiro, and S. B. Oseroff, Phys. Rev. B **60**, 11879 (1999).

[32]W. Hayes and R. A. Loudon, *Light Scattering by Crystals* (John Wiley & Sons Ltd., New York, 1978).

[33]M. J. Massey, N. H. Chen, J. W. Allen, and R. Merlin, Phys. Rev. B **42**, 8776 (1990).

[34]A. Sievers and M. Tinkham, Phys. Rev. **129**, 1566 (1963).

[35]E. Chung, D. Paul, G. Balakrishnan, M. Lees, A. Ivanov, and M. Yethiraj, Phys. Rev. B **68**, 140406 (2003).

[36]N. Mironova-Ulmane, A. Kuzmin, I. Steins, J. Grabis, I. Sildos, and M. Pärs, J. Phys.: Conf. Ser. **93**, 12039 (2007).

[37]M. G. Cottam, J. Phys. C: Solid State Phys. **5**, 1461 (1972).

[38]M. Press, M. Mayer, P. Knoll, S. Lo, U. Hohenester, and E. Holzinger-Schweiger, J. Raman Spectrosc. **27**, 343 (1996).

[39]R. J. Powell and W. E. Spicer, Phys. Rev. B **2**, 2182 (1970).

[40]G. A. Sawatzky and J. W. Allen, Phys. Rev. Lett. **53**, 2339 (1984).

[41]S. Di Sabatino, J. A. Berger, L. Reining, and P. Romaniello, Phys. Rev. B **94**, 155141 (2016).

[42]A. V. Chubukov and D. M. Frenkel, Phys. Rev. B **52**, 9760 (1995).

[43]A. Floris, S. de Gironcoli, E. K. U. Gross, and M. Cococcioni, Phys. Rev. B **84**, 161102 (2011).

[44]P. G. Klemens, Phys. Rev. **148**, 845 (1966).

[45]M. Balkanski, R. F. Wallis, and E. Haro, Phys. Rev. B **28**, 1928 (1983).

[46]A. B. Sushkov, O. Tchernyshyov, W. Ratcliff, S. W. Cheong, and H. D. Drew, Phys. Rev. Lett. **94**, 137202 (2005).

[47]S. Calder, J. H. Lee, M. B. Stone, M. D. Lumsden, J. C. Lang, M. Feygenson, Z. Zhao, J.-Q. Yan, Y. G. Shi, Y. S. Sun, Y. Tsujimoto, K. Yamaura, and A. D. Christianson, Nat. Commun. **6**, 8916 (2015).

[48]X. K. Chen, J. C. Irwin, and J. P. Franck, Phys. Rev. B **52**, R13130 (1995).

[49]N. Mironova-Ulmane, A. Kuzmin, I. Sildos, and M. Pärs, Open Phys. **9**, 1096 (2011).

[50]Y. Wang, J. E. Saal, J.-J. Wang, A. Saengdeejing, S.-L. Shang, L.-Q. Chen, and Z.-K. Liu, Phys. Rev. B **82**, 81104 (2010).

[51]A. Rohrbach, J. Hafner, and G. Kresse, Phys. Rev. B **69**, 075413 (2004).

[52]H. Uchiyama, S. Tsutsui, and A. Q. R. Baron, Phys. Rev. B **81**, 241103 (2010).

[53]R. Merlin, Journal De Physique **41**, C5–233 (1980).